












# Spectroscopy outperforms leaf trait relationships for predicting photosynthetic capacity across different forest types

Zhengbing Yan<sup>1</sup> , Zhengfei Guo<sup>1</sup>, Shawn P. Serbin<sup>2</sup> , Guangqin Song<sup>1</sup>, Yingyi Zhao<sup>1</sup>, Yang Chen<sup>1</sup>, Shengbiao Wu<sup>1</sup> , Jing Wang<sup>1</sup>, Xin Wang<sup>3</sup> , Jing Li<sup>3,4</sup>, Bin Wang<sup>3,4</sup> , Yuntao Wu<sup>3,4</sup> , Yanjun Su<sup>3,4</sup> , Han Wang<sup>5,6</sup> , Alistair Rogers<sup>2</sup> , Lingli Liu<sup>3,4</sup>  and Jin Wu<sup>1</sup> 

<sup>1</sup>Division for Ecology and Biodiversity, School of Biological Sciences, The University of Hong Kong, Pokfulam Road, Hong Kong, China; <sup>2</sup>Environmental & Climate Sciences Department, Brookhaven National Laboratory, Upton, NY 11973, USA; <sup>3</sup>State Key Laboratory of Vegetation and Environmental Change, Institute of Botany, Chinese Academy of Sciences, Xiangshan Beijing 100093, China; <sup>4</sup>University of Chinese Academy of Sciences, Yuquanlu Beijing 100049, China; <sup>5</sup>Ministry of Education Key Laboratory for Earth System Modelling, Department of Earth System Science, Tsinghua University, Beijing 100084, China; <sup>6</sup>Joint Centre for Global Change Studies, Tsinghua University, Beijing 100084, China

## Summary

Author for correspondence:

Jin Wu

Email: [jinwu@hku.hk](mailto:jinwu@hku.hk)

Received: 27 March 2021

Accepted: 20 June 2021

*New Phytologist* (2021) **232**: 134–147

doi: 10.1111/nph.17579

**Key words:** gas exchange, leaf hyperspectral reflectance, maximum carboxylation capacity, multitrait covariance, partial least-squares regression (PLSR), plant functional traits, vegetation spectroscopy.

- Leaf trait relationships are widely used to predict ecosystem function in terrestrial biosphere models (TBMs), in which leaf maximum carboxylation capacity ( $V_{c,max}$ ), an important trait for modelling photosynthesis, can be inferred from other easier-to-measure traits. However, whether trait– $V_{c,max}$  relationships are robust across different forest types remains unclear.
- Here we used measurements of leaf traits, including one morphological trait (leaf mass per area), three biochemical traits (leaf water content, area-based leaf nitrogen content, and leaf chlorophyll content), one physiological trait ( $V_{c,max}$ ), as well as leaf reflectance spectra, and explored their relationships within and across three contrasting forest types in China.
- We found weak and forest type-specific relationships between  $V_{c,max}$  and the four morphological and biochemical traits ( $R^2 \leq 0.15$ ), indicated by significantly changing slopes and intercepts across forest types. By contrast, reflectance spectroscopy effectively collapsed the differences in the trait– $V_{c,max}$  relationships across three forest biomes into a single robust model for  $V_{c,max}$  ( $R^2 = 0.77$ ), and also accurately estimated the four traits ( $R^2 = 0.75–0.94$ ).
- These findings challenge the traditional use of the empirical trait– $V_{c,max}$  relationships in TBMs for estimating terrestrial plant photosynthesis, but also highlight spectroscopy as an efficient alternative for characterising  $V_{c,max}$  and multitrait variability, with critical insights into ecosystem modelling and functional trait ecology.

## Introduction

An accurate understanding and representation of the relationships among plant traits has been an essential prerequisite to quantify their roles in determining key ecological processes, ranging from instantaneous physiological response and resource use to carbon allocation, long-term adaptation and community assembly (Wright *et al.*, 2004; Díaz *et al.*, 2016). Given their importance in shaping emergent ecosystem function, the process modelling community has started to include these processes and mechanisms by simultaneously representing multiple important traits and trait variability in ecosystem models (Rogers *et al.*, 2017a; Bonan & Doney, 2018; Berzaghi *et al.*, 2020). These representations of trait variability have been shown to improve simulations of ecosystem-scale resilience and the sensitivity to climate change (Bonan & Doney, 2018). As it is difficult to measure the full suite of leaf traits at the same time, but also redundant to incorporate many of these traits as they are highly correlated, empirical and well established leaf trait relationships, including

the worldwide leaf economics spectrum (Wright *et al.*, 2004; Díaz *et al.*, 2016), are often adopted in the ecosystem models. With leaf trait relationships, several important but difficult-to-measure traits (e.g. leaf life span and light saturated photosynthetic rate) can be indirectly inferred from other relatively easier-to-measure traits (e.g. leaf mass per area (LMA) and leaf nitrogen (N) content) with more extensive spatial coverage (Wright *et al.*, 2005; Reich *et al.*, 2007; Berzaghi *et al.*, 2020).

One of the most important but difficult-to-measure traits is the leaf maximum carboxylation rate of the enzyme RuBisCo standardised to a reference temperature of 25°C ( $V_{c,max25}$ ; Rogers *et al.*, 2017a).  $V_{c,max25}$  directly mediates biotic controls on whole-plant to canopy photosynthetic carbon uptake and interactions with climate (Kattge *et al.*, 2009; Wu *et al.*, 2016). In terrestrial biosphere models (TBMs),  $V_{c,max25}$  is an important biochemical parameter that regulates modelled leaf photosynthetic rate, and its parameterisation largely determines the accuracy of TBM simulations of terrestrial photosynthesis and carbon uptake (Bernacchi *et al.*, 2013; Rogers *et al.*, 2017a). However,

$V_{c,max25}$  also displays large variability in nature and is affected by multiple abiotic and biotic factors, such as climate conditions, soil properties, plant species, leaf morphology and leaf age (e.g. Walker *et al.*, 2014; Ali *et al.*, 2015; Albert *et al.*, 2018; Smith & Dukes, 2018; Wu *et al.*, 2019). Therefore, efficient and accurate estimation of  $V_{c,max25}$  variability across scales from individual organisms to forest ecosystems remains an essential step to improve the characterisation of the drivers of  $V_{c,max25}$  variability and the subsequent parameterisation and evaluation of TBMs.

At present,  $V_{c,max25}$  is parameterised in TBMs in a few different ways (Rogers, 2014). For example, the default approach for some models is to use a single static value for each discrete plant functional type (PFT), often parameterised with mean values for the PFT derived from the literature (Kattge *et al.*, 2009; Rogers, 2014; Berzaghi *et al.*, 2020). As an alternative to the fixed parameterisations, some groups have explored the capacity to develop custom parameterisations based on trait databases and statistical methods to derive the best estimate for each PFT (e.g. Lebauer *et al.*, 2013; Dietze *et al.*, 2014). Other approaches include a more direct parameterisation through model inversion, for example using eddy covariance-derived photosynthesis (gross primary productivity, GPP) (Zheng *et al.*, 2017; Schimel *et al.*, 2019) or satellite-based solar-induced chlorophyll fluorescence data (Zhang *et al.*, 2018; Camino *et al.*, 2019; L. M. He *et al.*, 2019) to tune  $V_{c,max25}$ . Others may instead build in a broad range of trait variance into simulations to explore which trait value combinations result in simulation more closely related to benchmarks, such as eddy covariance-derived GPP (Koven *et al.*, 2020). More recently, researchers have also explored the use of optimality approaches (e.g. Prentice *et al.*, 2014) that rely on the photosynthetic least-cost theory (Wright *et al.*, 2003) to infer  $V_{c,max25}$  given ambient climate conditions (Wang *et al.*, 2017; Smith *et al.*, 2019; Jiang *et al.*, 2020). These various approaches vary in their accuracy and remain limited to the estimation of  $V_{c,max25}$  at the ecosystem scale rather than at the individual organism level.

Alternatively, to capture the variability at the finer scale,  $V_{c,max25}$  is often indirectly inferred through its empirical relationships with other leaf traits, such as LMA (Kattge *et al.*, 2009; Walker *et al.*, 2014), leaf N content per unit leaf area ( $N_a$ ) (Kattge *et al.*, 2009; Walker *et al.*, 2014), chlorophyll (Chl) content (Croft *et al.*, 2017), and leaf phosphorus (P) content (Walker *et al.*, 2014; Norby *et al.*, 2017). However, as shown by many field-based studies, the empirical trait– $V_{c,max25}$  relationships can generate large uncertainties in characterising  $V_{c,max25}$  variability at the finer scale both within and across sites, because the trait– $V_{c,max25}$  relationships often vary with plant species, seasons, and plant growth environments (Domingues *et al.*, 2010; Serbin *et al.*, 2012; Prentice *et al.*, 2014; Dechant *et al.*, 2017; Norby *et al.*, 2017; Rogers *et al.*, 2017b). In addition, whether the trait– $V_{c,max25}$  relationships are robust across diverse PFTs remains unclear, and the combined measurements of both traits and  $V_{c,max25}$  over large geographical areas for this evaluation remain lacking. An exploration of the potential breakdown of trait– $V_{c,max25}$  relationships across various scales from tree individuals to contrasting forest types as well as an accurate and scalable alternative for consistent estimation of  $V_{c,max25}$  across scales remains critically needed.

Importantly, leaf reflectance spectroscopy or the measurement of reflected radiance from leaves in many narrow, continuous spectral channels across a portion of the electromagnetic spectrum (Serbin & Townsend, 2020), may fill an important role in enhancing our understanding of trait variation within and across Earth's terrestrial ecosystems. Leaf reflectance spectra are a collection of optical properties that are linked to a large number of leaf morphological and biochemical characteristics by electronic and vibrational absorption (Curran, 1989; Elvidge, 1990; Kokaly *et al.*, 2009). Given the strong connection between traits and reflectance spectra, a range of studies have demonstrated that leaf reflectance spectra can accurately estimate a broad suite of plant traits (e.g. leaf water content (LWC), LMA,  $N_a$ , leaf Chl and P contents, and leaf age) with high precision and accuracy, even despite strong variation in traits due to biotic and abiotic factors (Serbin *et al.*, 2014, 2019; Singh *et al.*, 2015; Asner *et al.*, 2016; 2017, 2019). Recent studies have also demonstrated that spectroscopy can accurately predict  $V_{c,max25}$  variability at some specific ecosystems/PFTs, but present research has been limited to relatively narrow sampling of woody plants or crop species that are often found in a single ecosystem (Serbin *et al.*, 2012; Dechant *et al.*, 2017; Meacham-Hensold *et al.*, 2019; Wu *et al.*, 2019). This leaves a fundamental but unanswered question: Is the spectroscopic approach an accurate and scalable means for  $V_{c,max25}$  estimation across various forest types spanning large environmental gradients?

The goal of this study was to evaluate the different approaches for predicting finer-scale  $V_{c,max25}$  variability both within and across diverse forest types, as well as to explore the possibility of a cross-site approach for inferring  $V_{c,max25}$  using leaf reflectance spectroscopy. Specifically, we addressed the following two questions: (1) Can empirical trait– $V_{c,max25}$  relationships hold up for predicting  $V_{c,max25}$  across forest types? and (2) Can leaf spectroscopy offer an efficient alternative to predict  $V_{c,max25}$  and represent trait– $V_{c,max25}$  relationships by accurately inferring both  $V_{c,max25}$  and other traits from leaf reflectance spectra? To address these questions, we collected a set of leaf traits and reflectance spectra of canopy trees from the three forest types, namely a temperate broad-leaved coniferous forest, a subtropical evergreen broad-leaved forest, and a tropical evergreen broad-leaved forest. We focused on four key leaf traits (i.e. LMA, LWC,  $N_a$  and leaf Chl content) that are of interest to the broad plant ecology community and have been shown to drive a large fraction of model simulation uncertainty in current ecosystem models (Wright *et al.*, 2004; Díaz *et al.*, 2016; Bonan & Doney, 2018; Ricciuto *et al.*, 2018). Through answering these questions, we hope this can advise a practical approach to capture the  $V_{c,max25}$  variability across various scales and improve the understanding of the relationships among leaf  $V_{c,max25}$ , traits and spectra both within and across forest types.

## Materials and Methods

### Study sites and plant materials

This study was conducted at three forest sites that represent contrasting vegetation types in China, including Mountain Changbai (CB; 42°24'N, 128°06'E), Mountain Dinghu (DH; 23°10'N,

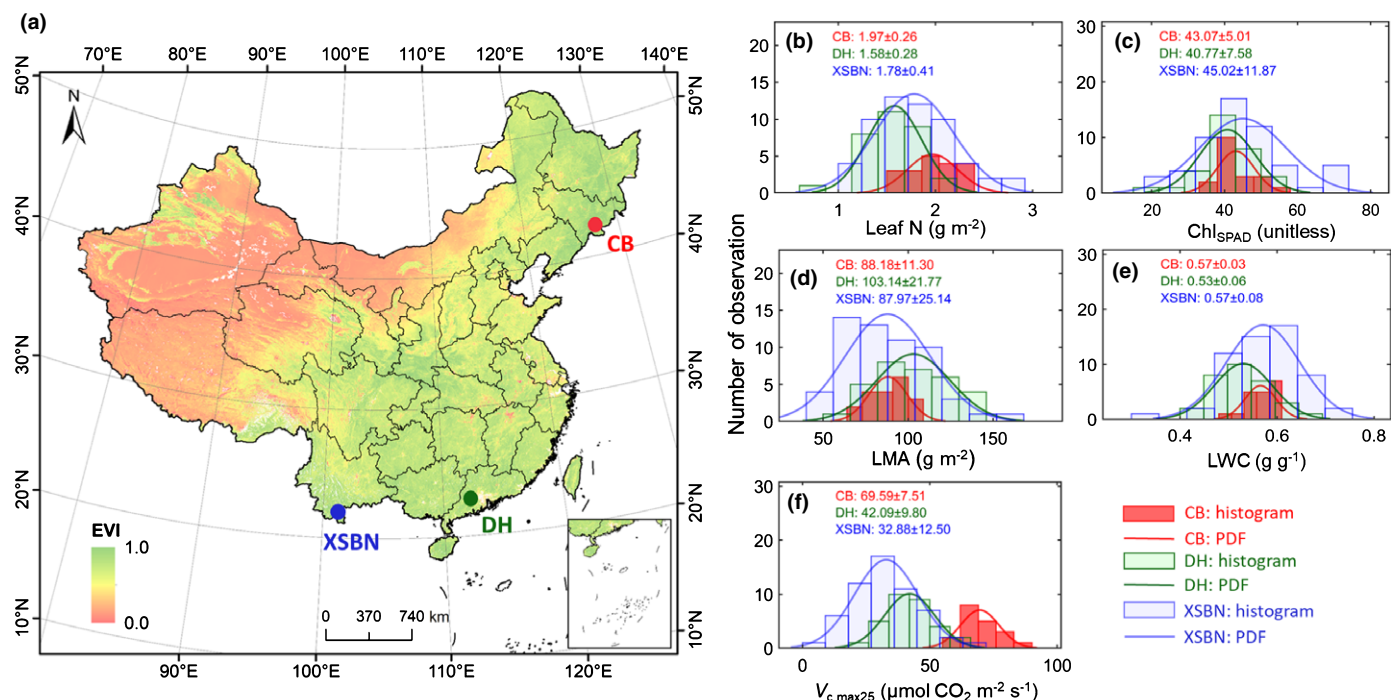


**Fig. 1** Sites and histogram distributions of leaf traits across the three forest types in China. (a) Location of the three canopy crane sites that span a large latitudinal gradient, including a temperate forest in Mountain Changbai (CB), a subtropical forest in Mountain Dinghu (DH), and a tropical rainforest in Xishuangbanna (XSBN). The background shows a map of mean enhanced vegetation index (EVI) in the 2019 peak growing season (July–August) derived from the MOD13A1 products. (b–f) Site-specific histogram distributions of maximum carboxylation rate of RuBisCo standardised to 25°C ( $V_{c,max25}$ ) and the other four leaf traits (i.e. leaf nitrogen (N) content, SPAD-based leaf chlorophyll content ( $Chl_{SPAD}$ ), leaf mass per area (LMA), leaf water content (LWC)), with CB in red, DH in green and XSBN in blue. The PDF shown in the figure legend refers to the probability distribution function (PDF) that was used to fit the site-specific histogram distribution. Numbers in the panel (b–f) are the mean  $\pm$  standard deviation of the trait values for each forest site.  $V_{c,max25}$  and leaf traits were sampled in the 2019 peak growing season, and trait values of individual tree means from all leaf ages are presented here.

112°32'E), and Xishuangbanna (XSBN; 21°47'N, 101°03'E) (Fig. 1a). At each site, the Chinese Academy of Sciences (CAS) maintains a canopy crane facility enabling access to a 1-hectare area of each forest, with the crane tower height of 40 m in CB, 60 m in DH and 81 m in XSBN. We selected these sites for two reasons. First, they represent dominant forest types (i.e. temperate, subtropical and tropical) in China. These sites cover large gradients in mean annual temperature and precipitation (i.e. 2.8°C and 691 mm yr<sup>-1</sup> in CB, 20.9°C and 1927 mm yr<sup>-1</sup> in DH, and 21.8°C and 1493 mm yr<sup>-1</sup> in XSBN) (Ye *et al.*, 2008; Shen *et al.*, 2018; N. P. He *et al.*, 2019) and soil types (i.e. from dark brown forest soil in CB to laterite soil in both DH and XSBN; see Supporting Information Table S1 for details on the variation in soil properties) (Cao *et al.*, 2006; Wu *et al.*, 2006; Gui *et al.*, 2019). These ensure our collected leaf traits and reflectance spectra span sufficient ranges caused by plant species and growth environments. Second, these sites have canopy crane facilities that allow easy access to the abundant canopy tree species that are representative of each forest type. Specifically, the abundant canopy tree species include *Pinus koraiensis*, *Tilia amurensis*, *Juglans mandshurica*, *Ulmus davidiana*, *Fraxinus mandshurica*, and other interspersed deciduous species in CB (Wu *et al.*, 2006; Liang & Liu, 2019); *Schima superba*, *Pinus massoniana*, *Castanopsis chinensis*, *Machilus breviflora*, and other interspersed evergreen broad-leaved species in DH (Ye *et al.*, 2008; Gui *et al.*, 2019); and *Parashorea chinensis*, *Canarium*

*album*, *Pometia tomentosa*, *Sloanea tomentosa* and *Semecarpus reticulata* and other interspersed evergreen broad-leaves species in XSBN (Cao *et al.*, 2006; Shen *et al.*, 2018).

Within the forest canopy crane footprint, 19 trees from seven dominant canopy tree species in CB, 31 trees from 12 dominant canopy tree species in DH, and 57 trees from 28 dominant canopy tree species in XSBN were selected (Table S2). Only upper canopy, sunlit leaves of these tree species were sampled and measured. Field measurements were conducted in the peak growing season (July–August) of 2019, including the measurements of leaf gas exchange, leaf reflectance spectra and four morphological and biochemical traits (i.e. LMA, LWC,  $N_a$  and leaf Chl content). Details of measurement protocols are shown below and the results of these measurements are summarised in Table S2. It is noteworthy that even if field measurements were conducted in the peak growing season, the leaf samples were still mixed with different leaf ages, especially in the subtropical and tropical forests. We therefore adopted the same approach as Wu *et al.* (2019) and classified the leaves into the two age categories (i.e. immature and mature leaves) according to the colour, size and rigidity of the leaves.

## Field measurements

**Leaf gas exchange and  $V_{c,max25}$**  Three portable gas exchange systems (LI-6400XT; Li-Cor Inc., Lincoln, NE, USA) were



used for leaf gas exchange measurements. The response of net  $\text{CO}_2$  assimilation rate ( $A$ ) to intracellular  $\text{CO}_2$  concentration ( $C_i$ ) (commonly known as the  $A$ – $C_i$  curve; e.g. Fig. S1) was measured on leaves from cut branches, which were sampled before dawn with water cut to avoid inducing xylem embolism when collecting branches (Wu *et al.*, 2019). The  $A$ – $C_i$  curves were measured closely following the protocol of Rogers *et al.* (2017b). Also see Methods S1 for details. For each tree, two branches were sampled and normally 1–3 leaves of all age classes (if present) per branch were measured. These field-derived  $A$ – $C_i$  curves were then fit to a biochemical photosynthesis model (Farquhar *et al.*, 1980), in which the modelled  $A$  best matched with the field-measured  $A$ , and therefore the leaf maximum carboxylation capacity ( $V_{c,\max}$ ) was derived for each  $A$ – $C_i$  curve. More details regarding the fitting procedure have been shown previously (Bernacchi *et al.*, 2013; Rogers *et al.*, 2017b; Wu *et al.*, 2019). We used the same code developed in MATLAB (Mathworks, Natick, MA, USA) by Wu *et al.* (2019) for the  $A$ – $C_i$  curve fitting, with example demonstrations shown in Fig. S1. Finally, the same kinetic constants and temperature response functions as Bernacchi *et al.* (2013) were used to standardise  $V_{c,\max}$  to a reference temperature of 25°C ( $V_{c,\max25}$ ). Admittedly, there is also an alternative approach for deriving  $V_{c,\max25}$  that accounts for the environmental acclimation of photosynthetic machinery (Kumarathunge *et al.*, 2019). We therefore cross-compared the two approaches, and found that  $V_{c,\max25}$  derived using the two approaches was almost identical (Fig. S2). As Bernacchi *et al.* (2013) has been widely used in previous trait– $V_{c,\max25}$  and spectral– $V_{c,\max25}$  analysis (e.g. Walker *et al.*, 2014; Rogers *et al.*, 2017b; Scafaro *et al.*, 2017; Wu *et al.*, 2019), we present our results based on that approach.

**Leaf reflectance spectra** Upon finishing gas exchange measurements, leaves were immediately measured for leaf reflectance spectra. A portable spectroradiometer Spectra Vista Corporation (SVC) HR-1024i (SVC, Poughkeepsie, NY, USA; spectral full-range: 350–2500 nm; spectral resolution:  $\leq 3.3$  nm at 700 nm,  $\leq 9.5$  nm at 1500 nm, and  $\leq 6.5$  nm at 2100 nm; sampling interval: linearly interpolated to 1 nm; Ely *et al.*, 2019) together with the SVC LC-RP-Pro foreoptic were used to measure leaf reflectance. During the spectral collection, the leaf reflectance probe used the internal calibrated light source to illuminate the samples with a black background, following the protocol of Wu *et al.* (2019). A 99% reflective Spectralon white panel by Labsphere Inc. (North Dutton, NH, USA) was used as the reference standard. The SVC was set to 1 s collection time (i.e. the integral scanning time for each spectrum collected was 1 s) with the spectrometer's automatic integration optimisation, to avoid the impacts of excessive heat loads on the data quality of leaf spectra collected (Serbin *et al.*, 2019). For each leaf, we measured the spectra on 3–6 different parts of the leaf adaxial surface (with only one spectrum of each part) depending on the leaf size, and used the averaged spectra to indicate the optical properties across all wavelengths. Additionally, we corrected the discontinuities in the spectra in the detector overlap areas using the vendor-provided SVC instrument software (Ely *et al.*, 2019). The

examples of collected leaf reflectance spectra are shown in Fig. S3 for demonstration.

**Leaf biochemical and morphological traits** After leaf spectral measurements, fresh leaf chlorophyll (Chl) content was estimated with a portable optical chlorophyll meter (SPAD-502 Plus; Konika-Minolta Inc., Tokyo, Japan). The SPAD value is an index based on the absorbance of the leaf at 650 and 940 nm (Uddling *et al.*, 2007), which has been shown as a good proxy for leaf Chl content in both crops and woody plants (Uddling *et al.*, 2007; Coste *et al.*, 2010; Silva-Perez *et al.*, 2018). We also compared the SPAD-based leaf Chl content with that inversed from a leaf-level radiative transfer model PROSPECT-5 with field-based spectral measurement as the model input, following the same approach as shown in Jacquemoud *et al.* (2009). These two proxies of leaf Chl content showed tight relationships ( $R^2 = 0.75$ ;  $P < 0.001$ ; Fig. S4), providing additional confidence on the use of the SPAD value to approximate fresh leaf Chl content in our leaf samples. We therefore used  $\text{Chl}_{\text{SPAD}}$  (unitless) that is short for SPAD-based leaf Chl content in this study.

Additionally, other three leaf traits were also derived, including LWC ( $\text{g g}^{-1}$ ), LMA ( $\text{g m}^{-2}$ ) and area-based leaf N content ( $\text{N}_a$ ;  $\text{g m}^{-2}$ ). Leaf area was measured using the cork borers, and leaf fresh mass was weighted using a precision balance (precision at 0.001 g; Meilen; Meifu Electronics Co. Ltd, Shenzhen, China) in a fixed location to reduce the impact of air movements. After that, the samples were oven dried to constant mass at 65°C for over 72 h, and then the dry mass was determined with the precision balance. LWC was calculated using the difference between leaf fresh and dry mass divided by leaf fresh mass. LMA was calculated using the leaf dry mass divided by leaf area. Dried leaves were then ground using a ball mill (NM200, Retsch, Haan, Germany) before measuring leaf N content. Mass-based leaf N content was analysed by the Dumas combustion method using an elemental analyser (Euro EA3028; EuroVector, Milan, Italy) coupled to a stable isotope ratio mass spectrometer (Perspective; Nu Instruments, Wrexham, UK) in continuous flow mode (EAIRMS). Area-based leaf N content was then calculated with the mass-based leaf N content multiplied by LMA. In terrestrial biosphere modelling researches, leaf N and  $V_{c,\max}$  are generally expressed on an area basis given that the main function of leaves is to intercept light (Osnas *et al.*, 2013; Walker *et al.*, 2014). Therefore, we restricted our following analyses to area-based leaf trait measurements.

## Data analysis

In this study, we focused on exploring the relationships of  $V_{c,\max25}$  with the four leaf traits and leaf spectra. Therefore, we chose leaf samples including all these measurements across the three forest sites. As a result, the dataset used for the analyses had 72 measurements in CB, 91 measurements in DH and 173 measurements in XSBN, respectively. The species-specific mean and range of  $V_{c,\max25}$  for all leaves across the three forest sites are presented in Table S2. We noted that our leaf samples from the tropical (XSBN) and subtropical (DH) forest types were mixed with different leaf age classes, with mature leaves ( $n = 281$ )

dominating over young leaves ( $n = 55$ ). To examine whether leaf age would affect the trait– $V_{c,max25}$  relationships, we performed a sensitivity analysis on the full dataset that respectively included (i.e. mature leaves only) or excluded (i.e. all leaves) the leaf age control. Our sensitivity analysis demonstrated that the results remained consistent regardless of with or without leaf age control (Figs S5, S6; Table S3). For clarity, we primarily focused on presenting the data analyses for the entire dataset without leaf age control thereafter.

**Exploring trait– $V_{c,max25}$  relationships within and across forest types** To explore the relationships between the four leaf traits and  $V_{c,max25}$  within and across forest types, we performed the three analyses. First, to explore the separate contribution of each trait on  $V_{c,max25}$  prediction, we analysed the relationships between  $V_{c,max25}$  and each of the four traits (i.e. LMA, LWC,  $Chl_{SPAD}$  and  $N_a$ ) using ordinary least-squares regression within and across forest types. Second, to explore the joint contribution of all the four traits on  $V_{c,max25}$  prediction, we performed a multiple linear regression analysis both within and across forest types. Third, to rank the independent, relative importance of each trait on  $V_{c,max25}$  prediction, we performed a principal component analysis (PCA) on all traits and  $V_{c,max25}$  with data from all forest types using the R package PRCOMP. All trait data were standardised using the zero-mean approach before the PCA analysis. The first two PCA axes were then plotted to visualise the trait space.

**Developing spectral models of  $V_{c,max25}$  and the four leaf traits** The partial least-squares regression (PLSR) approach (Serbin *et al.*, 2014) was used here to model the  $V_{c,max25}$  and the four traits (LWC, LMA,  $N_a$  and  $Chl_{SPAD}$ ) from leaf spectra within and across forest types. This PLSR method is commonly used in spectroscopic and chemometric analyses and has been shown to be superior to those classical regression approaches, give that it has the ability to handle high predictor collinearity and allow the number of predictor variables to be much higher compared with the number of observations (Ollinger & Smith, 2005; Serbin *et al.*, 2014, 2019; Asner *et al.*, 2016).

We adopted the same PLSR modelling approach as has been developed previously (Dechant *et al.*, 2017), in which the standard PLSR regression analysis was integrated with a repeated double cross-validation (rdCV) method (Filzmoser *et al.*, 2009). rdCV first splits the full dataset into calibration and independent validation subsets repeatedly using a cross-validation (outer CV loop), and then performed additional splits of each calibration subset into training and testing components using a cross-validation procedure (inner CV loop) to ensure that the optimal number of latent variables could be determined independently from the actual performance evaluation. Prediction performance is evaluated on the independent validation subsets (outer loop) over many possible random splits ( $n = 200$  in our case). This method therefore has the advantage to avoid the occurrence of good or bad results purely by chance.

Given that the model detail and settings have been shown in Dechant *et al.* (2017), we briefly summarised the five major steps of this approach below. First, we performed a square-root-

transformation on  $V_{c,max25}$  and the four traits to reduce the right-skewed frequency distribution of the original data for the PLSR analysis (Serbin *et al.*, 2019; Wu *et al.*, 2019). Second, we performed 200 repetitions for the rdCV and 10-fold cross-validation for both the outer and inner CV loops (Filzmoser *et al.*, 2009; Dechant *et al.*, 2017). Third, to avoid over-fitting, we determined the optimal latent variable number by maximising the averaged coefficient of determination ( $R^2$ ) and minimising the averaged root mean squares of error (RMSE) of the inner CV loop (Fig. S7). With the optimal PLSR latent variable number, we further derived the regression coefficients and variable importance in projection (VIP) metric (Wold *et al.*, 2001) for each permutation in the inner loop, and then averaged them to obtain the mean regression coefficients and VIP spectrum for each repetition. Fourth, we presented the mean and 95% confidence interval of PLSR regression coefficients and VIP metric generated by the 200 repetitions in the outer loop. This ensemble of PLSR model coefficients were ultimately used as the final model to predict  $V_{c,max25}$  or each trait plus the 95% confidence interval over the 200 repetitions. Fifth, the performance of the final PLSR model was evaluated using the independent validation subset for each of the 200 repetitions in the outer loop, measured by both  $R^2$  and RMSE (Fig. S8). For both  $V_{c,max25}$  and the four traits, all results were presented in the original units rather than the square-root-transformed units as the initial output of the PLSR model.

**Exploring spectral– $V_{c,max25}$  relationships under three spectral modelling scenarios** We performed the PLSR modelling of the three scenarios, with an aim to explore whether the spectral– $V_{c,max25}$  relationship can be extended to the cross-site scale. These three scenarios are summarised in Table 1 and illustrated as follows. First, a ‘site-specific’ spectral model of  $V_{c,max25}$  was developed and evaluated using all the data from each forest site. Second, a ‘XSBN’ spectral model of  $V_{c,max25}$  was developed and evaluated using all the data from the tropical forest site of XSBN only, and then the developed model was applied to the independent data from CB and DH. Third, a ‘cross-site’ spectral model of  $V_{c,max25}$  was developed and evaluated using the data from all three forest sites. By performing these modelling scenarios, it would not only improve our understanding of cross-site generalizability of spectral– $V_{c,max25}$  relationships, but also help to identify the potential scenarios in which spectra– $V_{c,max25}$  relationships might break down.

## Results

### Weak and decoupled relationships between $V_{c,max25}$ and leaf traits across forest types

To investigate our first question, trait-based approaches for  $V_{c,max25}$  predictions, we analysed the distribution of each leaf trait and  $V_{c,max25}$  (Fig. 1b–f) and then explored the trait– $V_{c,max25}$  relationships within and across forest types (Fig. 2). We found that the leaf morphological and biochemical traits and  $V_{c,max25}$  displayed a high degree of variation within and across forest types, with the tropical forest (XSBN) showing the largest spread in

**Table 1** Evaluation of the spectral- $V_{c,max25}$  model under the three scenarios: the 'site-specific model' (trained and evaluated using the data from each forest site through the repeated double cross-validation (rdCV) method), 'XSBN model' (trained and evaluated using the data from the tropical forest site of Xishuangbanna (XSBN) through the rdCV method, and then applied the model to the independent sites at Mountain Changbai (CB) and Mountain Dinghu (DH)), and 'cross-site model' (trained and evaluated using the data from all the three forest sites through the rdCV method).

Scenarios	Site	$V_{c,max25}$ ( $\mu\text{mol CO}_2 \text{ m}^{-2} \text{ s}^{-1}$ )		
		<i>n</i>	$R^2$	RMSE
Site-specific model	CB	72	0.28	9.9
	DH	91	0.55	9.5
	XSBN	173	0.59	10.3
	All	336	0.76	10.0
XSBN model	CB	72	0.20	10.4
	DH	91	0.48	10.2
	XSBN	173	0.59	10.3
	All	336	0.66	11.9
Cross-site model	CB	72	0.35	9.4
	DH	91	0.56	9.4
	XSBN	173	0.63	9.8
	All	336	0.77	9.7

*n*, sample size;  $R^2$ , the coefficient of determination; RMSE, the root mean square of error;  $V_{c,max25}$ , leaf maximum carboxylation rate of RuBisCo standardised to 25°C.

Leaf-level measurements across all leaf ages were analysed here. The three forest sites include the temperate forest in Mountain Changbai (CB), the subtropical forest in Mountain Dinghu (DH), and the tropical forest in Xishuangbanna (XSBN).

values, followed by the subtropical (DH) and temperate (CB) forests (Fig. 1b–f). We also found that the trait ranges of XSBN covered the full ranges of DH and CB in all traits except  $V_{c,max25}$  (Fig. 1b–f), and therefore XSBN had a significantly lower  $V_{c,max25}$  compared with CB ( $t = 19.85$ ,  $P < 0.001$ ; two-tailed Student's *t*-test) and DH ( $t = 4.84$ ,  $P < 0.001$ ; two-tailed Student's *t*-test).

Exploring the trait- $V_{c,max25}$  relationships further, we found that these relationships were weak overall with a high degree of variation in forest type-specific slope and intercept of the relationships (Fig. 2a–d; Table S3). Among these relationships,  $N_a$  showed the highest  $V_{c,max25}$  prediction across forest types ( $R^2 = 0.13$ ,  $P < 0.001$ ), followed by  $\text{Chl}_{\text{SPAD}}$  ( $R^2 = 0.05$ ,  $P < 0.001$ ), LWC ( $R^2 = 0.01$ ,  $P = 0.030$ ), and LMA ( $R^2 = 0.01$ ,  $P = 0.179$ ). PCA confirmed these patterns and illustrated that leaf N content had the strongest relationship with  $V_{c,max25}$ , followed by  $\text{Chl}_{\text{SPAD}}$  (Fig. 3). LMA and LWC were near-orthogonal to  $V_{c,max25}$  (Fig. 3), suggesting no clear relationships between these two traits and  $V_{c,max25}$ . In addition, for the univariate exploration, we also used a multiple linear regression model for explaining variation in  $V_{c,max25}$  (Fig. 2e). The results showed that these traits together explained slightly higher degrees of variation in  $V_{c,max25}$  across all the three contrasting forest types ( $R^2 = 0.15$ ; Fig. 2e) than models that relied on the univariate exploration (Fig. 2a–d). The results also showed higher predictive power of the multivariate model within each forest type, with  $R^2$  of 0.34, 0.30 and 0.19 for CB, DH and XSBN, respectively (Fig. 2e). In addition, our results

showed that the trait-based model when including the site effect (i.e. site-specific trait-based model) had the predictive power of  $R^2 = 0.61$ , which was much higher than its correspondence using the cross-site trait-based model ( $R^2 = 0.15$ ) (Fig. 2e).

### Spectroscopy outperforms leaf trait relationships for predicting $V_{c,max25}$ across forest types

To investigate our second question, on the spectral-based approach for reconciling the lower performance of the trait-based approach in explaining cross-site  $V_{c,max25}$  variability, we analysed the relationships between leaf traits/ $V_{c,max25}$  and spectra. We found that the cross-site spectral models accurately capture the variations in all traits, including  $V_{c,max25}$  ( $R^2 = 0.77$ , RMSE =  $9.7 \mu\text{mol CO}_2 \text{ m}^{-2} \text{ s}^{-1}$ ),  $N_a$  ( $R^2 = 0.79$ , RMSE =  $0.19 \text{ g m}^{-2}$ ),  $\text{Chl}_{\text{SPAD}}$  ( $R^2 = 0.92$ , RMSE = 3.2), LMA ( $R^2 = 0.93$ , RMSE =  $6.6 \text{ g m}^{-2}$ ), and LWC ( $R^2 = 0.93$ , RMSE = 0.021) (Figs 4, S9). These results demonstrated that leaf spectroscopy accurately predicted not only the four leaf biochemical and morphological traits but also the physiological trait of  $V_{c,max25}$  across the three contrasting forest types.

To explore the spectral- $V_{c,max25}$  relationships further, we conducted two additional tests, in which the spectral model of  $V_{c,max25}$  was calibrated for: (1) each forest site, and (2) tropical forest site only (XSBN). The site-specific spectral model of  $V_{c,max25}$  had the comparable predictive power with the cross-site model ( $R^2 = 0.76$  in Fig. 5a vs  $R^2 = 0.77$  in Fig. 4). The XSBN model had the worst performance ( $R^2 = 0.66$  in Fig. 5b), with a significant model bias when applied to the other two forest sites that were not involved in the model built (Fig. 5b; Table 1). Furthermore, we found that the cross-site model yielded the lowest prediction uncertainty as indicated by the horizontal error bars (Fig. 4 vs Fig. 5). These results collectively demonstrated that an accurate and cross-site scalable spectra- $V_{c,max25}$  relationship could be derived when sufficient leaf samples were involved in the model development.

## Discussion

This study has two main findings. First, we demonstrated that there were weak, forest type-specific trait- $V_{c,max25}$  relationships (Figs 1, 2). Second, we revealed that leaf spectroscopy collapsed this variability into a single spectral model that accurately predicted  $V_{c,max25}$  both within and across forest types (Fig. 4). Collectively, our study suggests that leaf spectroscopy outperforms trait- $V_{c,max25}$  relationships for predicting leaf photosynthetic capacity across three contrasting forest types in China.

Our observations of weak and forest type-specific trait- $V_{c,max25}$  relationships are consistent with many previous field-based studies, which also report moderate-to-weak trait- $V_{c,max25}$  relationships at the interspecies, intersite and inter-PFT level (Domingues *et al.*, 2010; Serbin *et al.*, 2012; Prentice *et al.*, 2014; Walker *et al.*, 2014; Rogers *et al.*, 2017b). In addition, our observed forest type-specific  $N_a$ - $V_{c,max25}$  relationship also agrees with a previous global-scale synthesis study, which shows that the slopes and intercepts of  $N_a$ - $V_{c,max25}$  relationships vary with PFTs

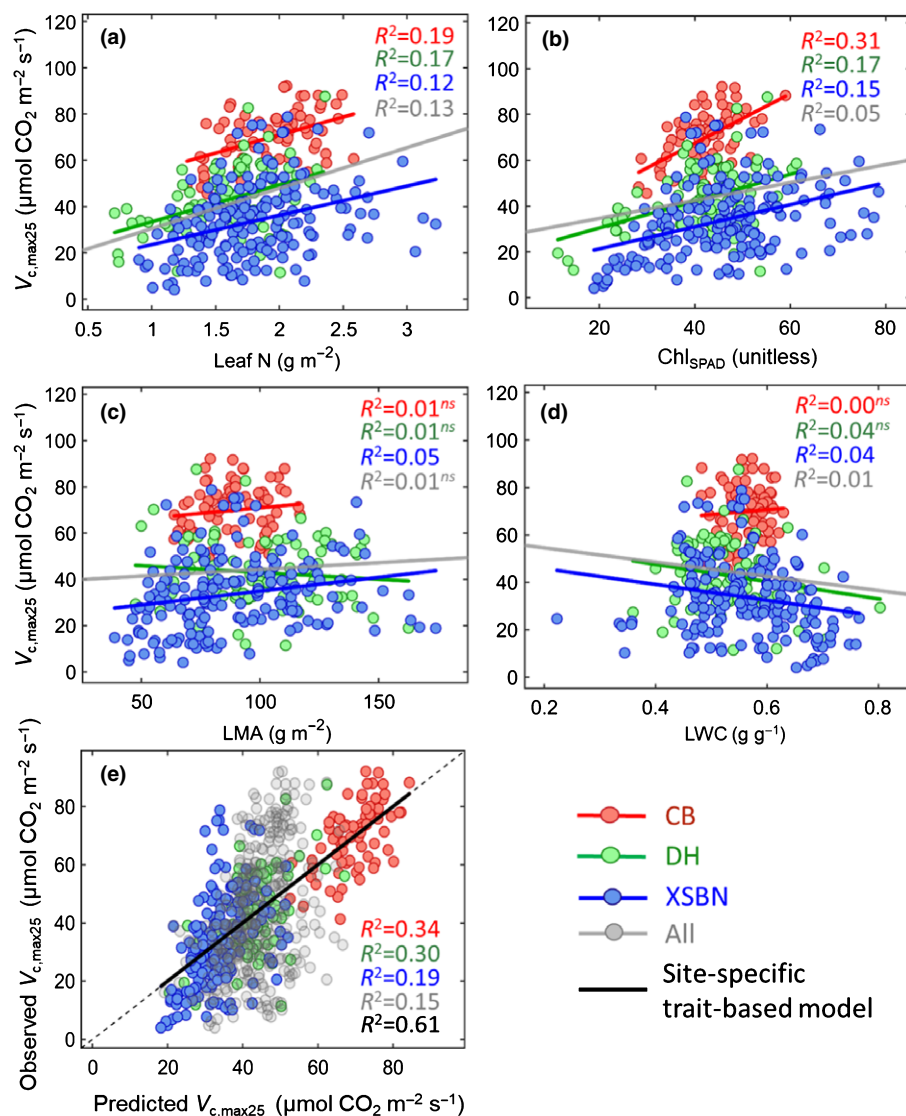


**Fig. 2** Exploring trait– $V_{c,max25}$  relationships both within and across forest types. (a–d) Pairwise relationship between leaf maximum carboxylation rate of RuBisCo standardised to 25°C ( $V_{c,max25}$ ) and the other four leaf traits (i.e. leaf nitrogen (N) content, SPAD-based leaf chlorophyll content ( $\text{Chl}_{SPAD}$ ), leaf mass per area (LMA), leaf water content (LWC)) within and across the three forest types. (e) Performance (observed vs. predicted  $V_{c,max25}$ ) of the multiple linear regression model using all four leaf traits as predictor variables. Three different coloured circles represent each of the three forest sites, with Mountain Changbai (CB) in red, Mountain Dinghu (DH) in green, and Xishuangbanna (XSBN) in blue. Lines were fitted by ordinary least-squares regressions, with coloured lines for site-specific regression fitting and the grey line for all-sites' regression fitting. In (e), the dashed line represents the 1 : 1 line, and the black line represents the regression fitting when combining the site-specific multiple linear regression model results.  $R^2$  represents the coefficient of determination; 'ns' denotes the insignificant relationship with  $P > 0.05$ . Leaf-level trait measurements across all leaf ages were involved in this analysis.

(i.e. tropical trees, temperate broad-leaved trees and coniferous trees) at the global scale (Kattge *et al.*, 2009). There are several possible explanations for this including variation in the fraction of  $N_a$  allocated to RuBisCo and variation in mesophyll conductance, which both affect the ratio between  $N_a$  and  $V_{c,max25}$  (Ghimire *et al.*, 2017; Evans, 2021). As a result, the  $N_a$ – $V_{c,max25}$  relationship has been observed to vary with species, growth environments and PFTs, with  $N_a$  alone explaining a relatively low degree of  $V_{c,max25}$  variance at the global scale (Walker *et al.*, 2014; Ali *et al.*, 2015; Smith *et al.*, 2019). Despite the weak  $N_a$ – $V_{c,max25}$  relationship observed here and previously, this relationship remains widely used in TBMs to first infer  $V_{c,max25}$  and then

to simulate plant photosynthesis (Kattge *et al.*, 2009; Rogers *et al.*, 2017a). Our results, together with these previous studies, therefore raised concerns over implementing  $N_a$ – $V_{c,max}$  relationships in TBMs for modelling large-scale terrestrial photosynthesis and associated vegetative responses to the current and changing climate.

In addition to the weak  $N_a$ – $V_{c,max25}$  relationships, we observed the similarly weak and forest type-specific  $\text{Chl}$ – $V_{c,max25}$  relationships (using either  $\text{Chl}_{SPAD}$  or PROSPECT-5 inverted  $\text{Chl}$ ; Figs 2b, S4b). Our result is consistent with Luo *et al.* (2019) who also found the PFT-dependent  $\text{Chl}$ – $V_{c,max25}$  relationships based on previous studies with direct field measurements of  $\text{Chl}$  and



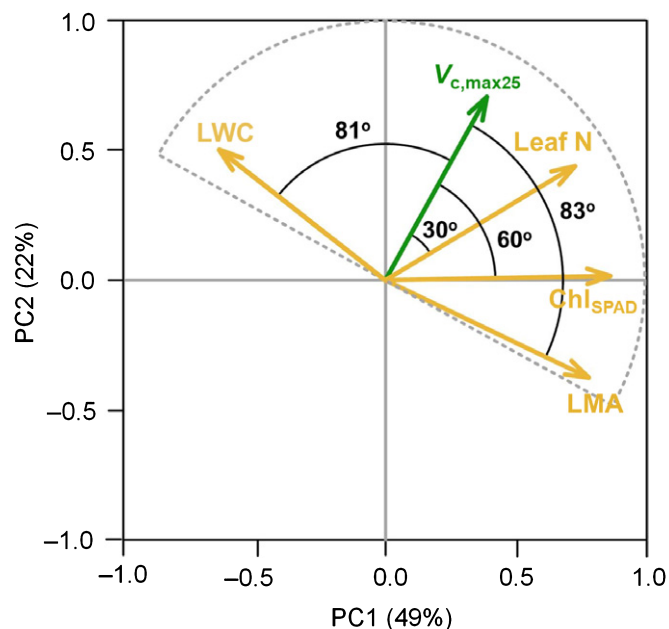


**Fig. 3** Exploring the cross-site trait– $V_{c,max25}$  relationships using principal component analysis. The trait loading on the plane below is defined by principal component 1 (PC1) and principal component 2 (PC2), with the green arrow for leaf maximum carboxylation rate of RuBisCo standardised to 25°C ( $V_{c,max25}$ ) and brown arrows for the other four leaf traits (i.e. leaf nitrogen (N) content, SPAD-based leaf chlorophyll content ( $Chl_{SPAD}$ ), leaf mass per area (LMA), leaf water content (LWC)). PC1 and PC2, respectively, explained 49% and 22% of total variation in all four traits and  $V_{c,max25}$ . The angle between  $V_{c,max25}$  and each of the four traits indicated the extent of correlation between them, with the smaller angle representing the higher correlation, and the 90° indicating the orthogonal relationship. Based on this analysis,  $V_{c,max25}$  shows higher relationship with leaf N content, followed by  $Chl_{SPAD}$ , but has nearly orthogonal relationships with LWC and LMA. In addition, all leaf traits are located within the grey semicircle region of  $V_{c,max25}$ , suggesting that all these trait– $V_{c,max25}$  relationships are positive. Leaf-level trait measurements across all ages and forest types were used in this analysis.

$V_{c,max25}$  across PFTs and use these PFT-specific relationships, together with satellite-derived leaf chlorophyll content, to estimate  $V_{c,max25}$  at the global-scale. Taken together, these results suggest that it is important to account for PFT-specific  $Chl$ – $V_{c,max25}$  relationships when leveraging field-derived and/or satellite-derived  $Chl$  measurements for large-scale  $V_{c,max25}$  prediction. Admittedly, both  $Chl_{SPAD}$  and PROSPECT-5 inverted  $Chl$  used in this study are indirect  $Chl$  measurements and, therefore, our  $Chl_{SPAD}$ – $V_{c,max25}$  relationship might not be directly applicable to those  $Chl$ – $V_{c,max25}$  studies relying on direct  $Chl$  measurements (e.g. Croft *et al.*, 2017; Chou *et al.*, 2020). However, our results suggest that global-scale studies in which satellite-derived leaf  $Chl$  content (comparable with our PROSPECT-5 inverted  $Chl$ ) is used in combination with ground-derived  $Chl$ – $V_{c,max25}$  relationships may mask marked variation in  $V_{c,max25}$  within and among forest types (Alton, 2017; Luo *et al.*, 2019; Croft *et al.*, 2020). We recommend that direct  $Chl$  measurements, satellite-derived  $Chl$  measurements, combined with  $V_{c,max25}$  and spectra data, across different PFTs are still needed to confirm our observations that relied on the two indirect  $Chl$  metrics.

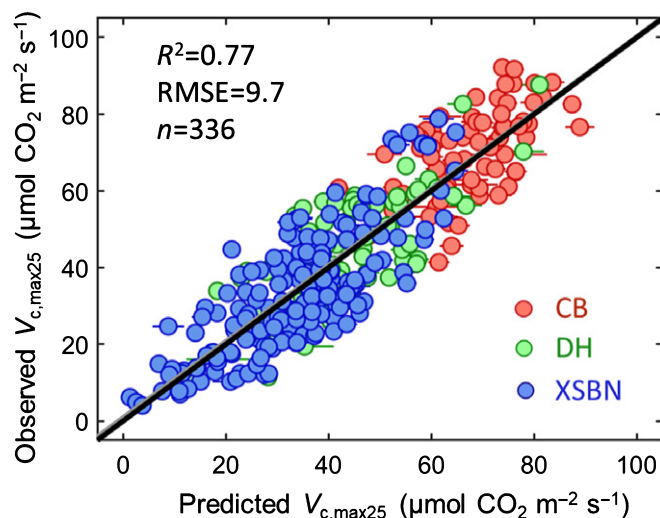


**Fig. 4** Accuracy assessment for the cross-site spectral– $V_{c,max25}$  relationship. The ‘cross-site’ spectral model of leaf maximum carboxylation rate of RuBisCo standardised to 25°C ( $V_{c,max25}$ ) was trained and evaluated using the data from all the three forest sites through the repeated double cross-validation method. Error bars indicate the 95% confidence intervals for each predicted value derived from the ensemble partial least-squares regression (PLSR) models (i.e. each PLSR model is represented by a set of PLSR fitted spectral coefficients averaged over the 200 repetitions). The grey line represents the ordinary least-squares regression fit, and the black line indicates the 1 : 1 line. Three different coloured circles represent each of the three forest sites, with Mountain Changbai (CB) in red, Mountain Dinghu (DH) in green, and Xishuangbanna (XSBN) in blue. Leaf-level trait measurements across all leaf ages were involved in this analysis.  $n$ , sample size;  $R^2$ , the coefficient of determination; RMSE, the root mean square of error.

If empirical trait– $V_{c,max25}$  relationships do not hold up for accurate and scalable predictions of  $V_{c,max25}$  across forest types, what is an alternative? Our answer is leaf spectroscopy, as a single spectral model accurately predicted  $V_{c,max25}$  across all three forest types ( $R^2 = 0.77$ ; Fig. 4). To the best of our knowledge, this represents the first study demonstrating the cross-site scalability of  $V_{c,max25}$  prediction using leaf spectroscopy. Also because Wu *et al.* (2019) demonstrated leaf spectroscopy as an accurate means for characterising the seasonal variability in  $V_{c,max25}$  across multiple tropical forests, leaf spectroscopy are, therefore, likely to be an accurate and scalable means for predicting  $V_{c,max25}$  across both large spatial and temporal extents. Additionally, our results of the cross-site tight covariations between leaf spectra and the four traits (Fig. S9) also confirmed the two very recent studies in which leaf spectroscopy accurately inferred key leaf biochemical and morphological traits (e.g.  $N_a$ , LMA, leaf carbon content and leaf total phenol content) across diverse forest types (Nakaji *et al.*, 2019; Serbin *et al.*, 2019). These together further suggest that leaf spectroscopy offers a promising and scalable means for monitoring leaf traits across various forest types, and that the measurement of leaf spectra alone together with a suitable PLSR model can accurately infer multiple leaf morphological, biochemical and physiological traits.

Our results further demonstrated that the cross-site scalable spectral– $V_{c,max25}$  relationship can be derived only when leaf



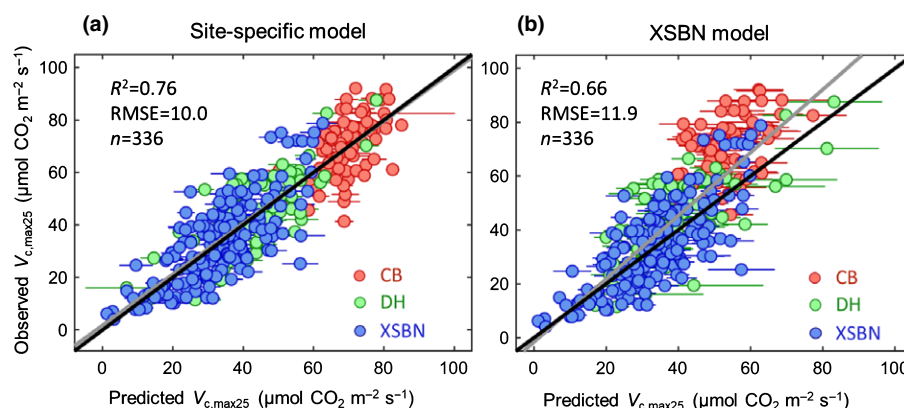


**Fig. 5** Accuracy assessments for the spectral models of leaf maximum carboxylation rate of RuBisCo standardised to 25°C ( $V_{c,max25}$ ) under the site-specific and Xishuangbanna (XSBN) scenarios. (a) 'Site-specific model' (trained and evaluated using the data from each forest site through the repeated double cross-validation (rdCV) method). (b) 'XSBN model' (trained and evaluated using the data from the tropical forest site of XSBN through the rdCV method, and then applied the model to the independent sites at Mountain Changbai (CB) and Mountain Dinghu (DH)). Error bars indicate the 95% confidence intervals for each predicted value derived from the ensemble partial least-squares regression (PLSR) models. The grey line represents the ordinary least-squares regression fit, and the black line indicates the 1 : 1 line. Three different coloured circles represent each of the three forest sites, with CB in red, DH in green and XSBN in blue. Leaf-level trait measurements across all leaf ages were used here.  $n$ , sample size;  $R^2$ , the coefficient of determination; RMSE, the root mean square of error.

samples covering sufficiently wide variability in both  $V_{c,max25}$  and spectra are involved in the model development (Figs 4, 5; Schweiger, 2020). Therefore, the prerequisite for developing a general and broadly applicable spectral model of  $V_{c,max25}$  is to encompass the full trait space associated with both physiological and spectral variation in the training dataset. Many observational studies have suggested that both leaf spectra and  $V_{c,max25}$  vary considerably among ecosystems (e.g. grasslands, shrublands and forests), climate zones (e.g. boreal, temperate, subtropical and tropical zones), life forms (e.g. evergreen and deciduous trees, coniferous and broad-leaved trees), leaf ages (e.g. young, mature and old leaves) and continents (e.g. China, Europe and North America) (Kattge *et al.*, 2009; Ali *et al.*, 2015; Dechant *et al.*, 2017; Albert *et al.*, 2018; Smith & Dukes, 2018; Wang *et al.*, 2018; Serbin *et al.*, 2019; Wu *et al.*, 2019). However, most of these variabilities are currently either undersampled or not sampled in our study. Therefore, further global sampling and analysis is still needed to explore and build a globally applicable spectral model of  $V_{c,max25}$  as that has been developed for LMA (Serbin *et al.*, 2019).

To elucidate the potential mechanism of spectral– $V_{c,max25}$  relationships, we explored the spectral regions that dominate the links between spectra and  $V_{c,max25}$  by analysing the patterns in the PLSR regression coefficients (Fig. 6a) and VIP (Fig. 6b). Our results showed that the reflectance contribution to the estimation of  $V_{c,max25}$  varied considerably across the full spectrum (Fig. 6a, b). Specifically, we found that the spectral domains of importance (i.e. VIP value > 0.8; Wold *et al.*, 2001) cover the visible range (450–700 nm), a strong response in the red-edge range (700–800 nm), and multiple near-infrared (NIR) (1030–1120 nm) and shortwave infrared (SWIR) bands (1350–1480 nm, 1640–1760 nm and 1820–2180 nm). These identified  $V_{c,max25}$ -sensitive spectral domains not only agree closely with several previous similar efforts that analyse the spectral– $V_{c,max25}$

relationships (Serbin *et al.*, 2012; Meacham-Hensold *et al.*, 2019; Wang *et al.*, 2020), but are also consistent with many other studies that broadly examined the relationship between reflectance spectra and leaf biochemistry and physiology (Curran, 1989; Elvidge, 1990; Kokaly *et al.*, 2009; Ustin *et al.*, 2009). For example, the visible range has been related to the concentration of leaf pigments (e.g. chlorophyll, carotenoids and anthocyanins; Wang *et al.*, 2020; also see Fig. 6e,f), the red-edge range has been associated with leaf Chl content (Fig. 6e,f), chlorophyll fluorescence emission, and photosystem II function (Zarco-Tejada *et al.*, 2000; Serbin *et al.*, 2012; Wang *et al.*, 2020), and the detected NIR and SWIR bands have been found tightly connected with leaf N and protein contents (Curran, 1989; Kokaly *et al.*, 2009; also see Fig. 6c,d) as well as leaf water and dry matter contents (Elvidge, 1990; Jacquemoud *et al.*, 2009; also see Fig. 6g–j). These observed  $V_{c,max25}$ -sensitive spectral regions, together with the previous understanding of trait-specific sensitive spectral regions, therefore support the trait-based hypothesis suggested by Wu *et al.* (2019) that  $V_{c,max25}$  is tightly connected with multiple leaf traits retrievable from leaf spectra as a candidate mechanism for the observed tight spectral– $V_{c,max25}$  relationship (Fig. 4).

The four leaf traits measured here explain a much smaller fraction of the variation in  $V_{c,max25}$  compared with the spectral model (15% vs 77%; Fig. 2e vs Fig. 4). Therefore, our results suggested that there are likely to be other unmeasured traits that aid in the determination of the cross-site variability in  $V_{c,max25}$ , and that information about those traits is present in the leaf spectra. These unmeasured traits or states might include leaf P content, leaf magnesium content, leaf temperature and leaf age (Walker *et al.*, 2014; Asner *et al.*, 2016; Wu *et al.*, 2019; Khan *et al.*, 2020; Wang *et al.*, 2020), but the direct quantitative evidence is currently missing. In addition, we observed that accounting for site-specific trait– $V_{c,max25}$  relationships largely improved  $V_{c,max25}$  prediction ( $R^2 = 0.15$  vs 0.61; Fig. 2e) while there was

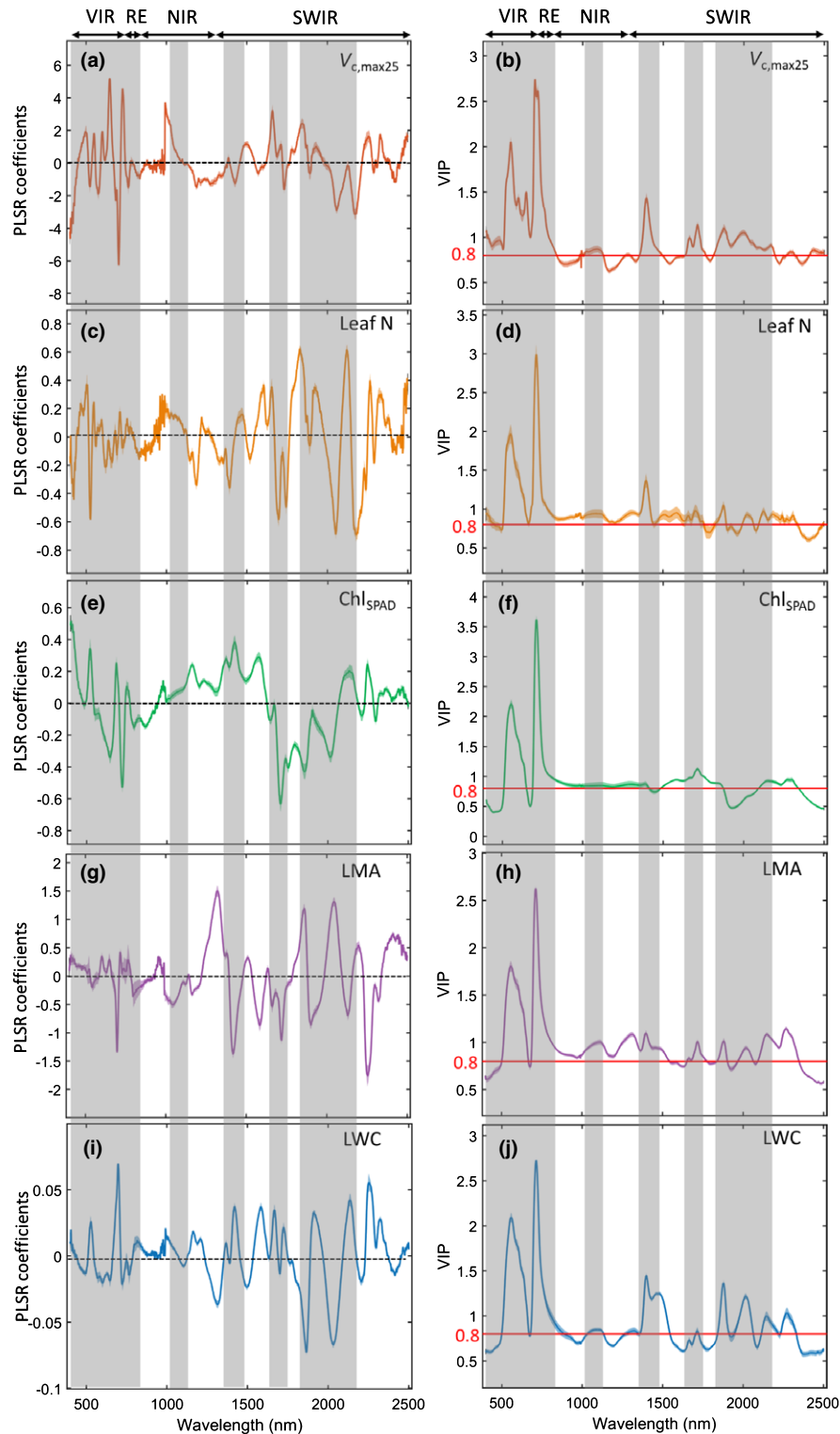


**Fig. 6** Assessing the reflectance contributions to the spectral models of leaf maximum carboxylation rate of RuBisCo standardised to 25°C ( $V_{c,max25}$ ) and the four leaf traits (i.e. leaf nitrogen (N) content, SPAD-based leaf chlorophyll content ( $Chl_{SPAD}$ ), leaf mass per area (LMA), leaf water content (LWC)) under the cross-site scenario using the partial least-squares regression (PLSR) approach, including the left panel (a, c, e, g, i) for PLSR regression coefficients, and the right panel (b, d, f, h, j) for the variable importance in projection (VIP). The cross-site spectral models were trained and evaluated using the data from all the three forest sites through the repeated double cross-validation method. The central coloured lines indicate the mean values and the shaded regions indicate the 95% confidence interval of PLSR regression coefficients and VIP spectrum, respectively. On the right panel,  $VIP \geq 0.8$  refers to the important spectral regions responsible for the spectral modelling of  $V_{c,max25}$  and the four leaf traits (Wold *et al.*, 2001). The shaded grey regions across all subpanels identify the corresponding spectral bands for the  $V_{c,max25}$  predictions. VIR, visible range (450–700 nm); RE, red-edge range (700–800 nm); NIR, near-infrared range (800–1300 nm); SWIR, shortwave infrared range (1300–2500 nm).

virtually no change in the spectral– $V_{c,max25}$  relationships between the cross-site model and site-specific model ( $R^2 = 0.77$  vs  $0.76$ ; Figs 4, 5a). These results further suggest that leaf spectra are able to capture the site-specific trait– $V_{c,max25}$  relationships and, therefore, a single spectral model consistently and accurately predicts  $V_{c,max25}$  across the three studied forest types. Site-specific trait– $V_{c,max25}$  relationships have often been attributed to environmental acclimation of  $V_{c,max25}$  to growth temperature and other abiotic conditions (e.g. light, water, and soil properties and nutrients) (Kattge *et al.*, 2009; Prentice *et al.*, 2014; Kumarathunge *et al.*, 2019; Smith *et al.*, 2019), yet leaf spectra have also been shown to capture or rapidly respond to changes in growth environment (Serbin *et al.*, 2012; Khan *et al.*, 2020). This suggests that spectra can adapt to the underlying trait modifications in response to their environmental acclimation over both short-term and long-term environmental changes. Therefore, it provides additional evidence that reflectance spectra can capture the site-specific variation in trait– $V_{c,max25}$  relationships associated with environmental acclimation. Regardless, an in-depth exploration of the spectral– $V_{c,max25}$  relationships, using experimental manipulations and measurements of more leaf traits,  $V_{c,max25}$ , and leaf spectra at both spatial and temporal (e.g. leaf age or seasonal) scales, is still needed to fully elucidate the underlying mechanism that enables successful prediction of  $V_{c,max25}$  from leaf spectra.

With these findings, our work also generated at least two implications as follows. First, our findings can complement current trait-based plant ecology studies. Empirical leaf trait relationships, regardless of their predictive strength, have been extensively used for reducing trait dimension and understanding plant adaptive strategies in functional ecology studies (Wright *et al.*, 2004; Díaz *et al.*, 2016). Our findings of the inconsistent leaf trait relationships across forest types suggest that the canonical leaf trait coordination theory (e.g. leaf economics spectrum that emphasises the convergent leaf trait relationships) (Wright *et al.*, 2004; Díaz *et al.*, 2016) works at the global scale, but breaks down at finer scales (Niinemets *et al.*, 2015; Anderegg *et al.*, 2018; Shiklomanov *et al.*, 2020). As leaf spectroscopy is able to accurately derive multiple leaf traits (Figs 4, S9) and leaf trait relationships (Fig. S10), it therefore offers a new way to characterise multitrait variability and improve representations of leaf trait relationships (including those weak relationships) in TBMs and functional ecology studies.

Second, our findings also have important implications for future work that aims to characterise the  $V_{c,max25}$  variability over large scales by leveraging leaf spectroscopy techniques. Our work suggests that leaf spectroscopic approaches can provide accurate, rapid, relatively low-cost and nondestructive estimates of  $V_{c,max25}$  across diverse plant species and forest types, which can facilitate the broader characterisation of  $V_{c,max25}$  variability that is useful for ecological research and process modelling. Moving up in scale from leaves to landscapes, as well as whole-ecosystems, using remote sensing data depends on the effective extension of results such as those presented here to vegetation canopies. Past research in agricultural landscapes suggests that this scaling up is possible using similar approaches (Serbin *et al.*, 2015), however additional

work is needed to develop generalised, robust methods. Importantly, canopy spectral variability is fundamentally tied to both leaf spectra and canopy structural attributes (e.g. leaf area index and leaf angle distribution) (Asner, 1998; Roberts *et al.*, 2004; Ollinger, 2011). At the same time, other challenges to spaceborne retrieval of  $V_{c,max25}$  are associated with a multitude of issues, including sensor design, uncertainties in the retrieval of surface reflectance, the sun-sensor geometry effect, and the mixture effect associated with the spatial resolution issue (Roberts *et al.*, 2004; Thompson *et al.*, 2019; Serbin & Townsend, 2020). Therefore, additional research is needed to understand the impacts of these issues on satellite retrievals of  $V_{c,max25}$ , yet new opportunities in spaceborne image spectroscopy could yield new insights (Guanter *et al.*, 2015; Stavros *et al.*, 2017; Schimel & Poulter, 2021). In addition, other novel platforms, including unoccupied aerial systems, may also provide new opportunities for developing large-scale maps of  $V_{c,max25}$  (Singh *et al.*, 2015; Asner *et al.*, 2016).

## Acknowledgements

J Wu, ZY, ZG, GS, YZ, YC, SW, and J Wang were supported by National Natural Science Foundation of China (nos. 31922090, 31901086), the Research Grants Council Early Career Scheme (no. 27306020) and Seed Fund for Basic Research (no. 201905159005). ZY was in part supported by the Division of Ecology and Biodiversity PDF research award. AR and SPS were supported by the Next-Generation Ecosystem Experiments (NGEE Tropics) project that is supported by the Office of Biological and Environmental Research in the Department of Energy, Office of Science, and through the United States Department of Energy contract (no. DE-SC0012704) to Brookhaven National Laboratory. The authors would like to thank the National Forest Ecosystem Research Stations at Xishuangbanna, Guanhua Dai and Jinlong Dong for canopy crane access assistance, thanks to Leung Kit Sum for providing help in laboratory chemical analyses of leaf samples, and thanks to the editor and the three anonymous reviewers for providing valuable suggestions and comments, which were greatly helpful in improving this manuscript.





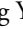
## Author contributions

JWu, ZY, SPS, AR and LL conceived the project idea; JWu and ZY designed the study; ZY, ZG, GS, YZ, YC, XW, JL, BW, YW and JWu collected the field data; ZY, ZG, SW, JWang and JWu performed the synthetic data analysis; SPS, YS, HW, AR and LL contributed to the result interpretation; ZY and JWu drafted the manuscript and all authors contributed to the final version.

## ORCID

Lingli Liu  <https://orcid.org/0000-0002-5696-3151>  
Han Wang  <https://orcid.org/0000-0003-2482-1818>  
Shengbiao Wu  <https://orcid.org/0000-0003-4569-6366>  
Alistair Rogers  <https://orcid.org/0000-0001-9262-7430>  
Shawn P. Serbin  <https://orcid.org/0000-0003-4136-8971>  
YanJun Su  <https://orcid.org/0000-0001-7931-339X>



Bin Wang  <https://orcid.org/0000-0003-0893-0539>  
 Xin Wang  <https://orcid.org/0000-0002-5274-7566>  
 Jin Wu  <https://orcid.org/0000-0001-8991-3970>  
 Yuntao Wu  <https://orcid.org/0000-0001-6505-1851>  
 Zhengbing Yan  <https://orcid.org/0000-0002-5028-8167>

## Data availability

The data that support the findings of this study are available from the corresponding author upon reasonable request.

## References

- Albert LP, Wu J, Prohaska N, Camargo PB, Huxman TE, Tribuzy ES, Ivanov VY, Oliveira RS, Garcia S, Smith MN *et al.* 2018. Age-dependent leaf physiology and consequences for crown-scale carbon uptake during the dry season in an Amazon evergreen forest. *New Phytologist* 219: 870–884.
- Ali AA, Xu C, Rogers A, McDowell NG, Medlyn BE, Fisher RA, Wullschlegel SD, Reich PB, Vrugt JA, Bauerle WL *et al.* 2015. Global-scale environmental control of plant photosynthetic capacity. *Ecological Applications* 25: 2349–2365.
- Alton PB. 2017. Retrieval of seasonal Rubisco-limited photosynthetic capacity at global FLUXNET sites from hyperspectral satellite remote sensing: impact on carbon modelling. *Agricultural and Forest Meteorology* 232: 74–88.
- Anderegg LDL, Berner LT, Badgley G, Sethi ML, Law BE, HilleRisLambers J. 2018. Within-species patterns challenge our understanding of the leaf economics spectrum. *Ecology Letters* 21: 734–744.
- Asner GP. 1998. Biophysical and biochemical sources of variability in canopy reflectance. *Remote Sensing of Environment* 3: 234–253.
- Asner GP, Knapp DE, Anderson CB, Martin RE, Vaughn N. 2016. Large-scale climatic and geophysical controls on the leaf economics spectrum. *Proceedings of the National Academy of Sciences, USA* 113: E4043–E4051.
- Bernacchi CJ, Bagley JE, Serbin SP, Ruiz-Vera UM, Rosenthal DM, Vanlooche A. 2013. Modelling C<sub>3</sub> photosynthesis from the chloroplast to the ecosystem. *Plant, Cell & Environment* 36: 1641–1657.
- Berzaghi F, Wright IJ, Kramer K, Oddou-Muratorio S, Bohn FJ, Reyer CPO, Sabaté S, Sanders TGM, Hartig F. 2020. Towards a new generation of trait-flexible vegetation models. *Trends in Ecology and Evolution* 35: 191–205.
- Bonan GB, Doney SC. 2018. Climate, ecosystems, and planetary futures: the challenge to predict life in Earth system models. *Science* 359: eaam8328.
- Camino C, Gonzalez-Dugo V, Hernandez P, Zarco-Tejada PJ. 2019. Radiative transfer  $V_{\text{cmax}}$  estimation from hyperspectral imagery and SIF retrievals to assess photosynthetic performance in rainfed and irrigated plant phenotyping trials. *Remote Sensing of Environment* 231: 111186.
- Cao M, Zou XM, Warren M, Zhu H. 2006. Tropical forests of Xishuangbanna, China. *Biotropica* 38: 306–309.
- Chavana-Bryant C, Malhi Y, Wu J, Asner GP, Anastasiou A, Enquist BJ, Cosio Caravasi EG, Doughty CE, Saleska SR, Martin RE *et al.* 2017. Leaf aging of Amazonian canopy trees as revealed by spectral and physiochemical measurements. *New Phytologist* 214: 1049–1063.
- Chavana-Bryant C, Malhi Y, Anastasiou A, Enquist BJ, Cosio EG, Keenan TF, Gerard FF. 2019. Leaf age effects on the spectral predictability of leaf traits in Amazonian canopy trees. *Science of the Total Environment* 666: 1301–1315.
- Chou SR, Chen B, Chen J, Wang MM, Wang SQ, Croft H, Shi Q. 2020. Estimation of leaf photosynthetic capacity from the photochemical reflectance index and leaf pigments. *Ecological Indicators* 110: 105867.
- Coste S, Baraloto C, Leroy C, Marcon E, Renaud A, Richardson AD, Roggy JC, Schimann H, Uddling J, Hérault B. 2010. Assessing foliar chlorophyll contents with the SPAD-502 chlorophyll meter: a calibration test with thirteen tree species of tropical rainforest in French Guiana. *Annals of Forest Science* 67: 607.
- Croft H, Chen JM, Luo XZ, Bartlett P, Chen B, Staebler RM. 2017. Leaf chlorophyll content as a proxy for leaf photosynthetic capacity. *Global Change Biology* 23: 3513–3524.
- Croft H, Chen JM, Wang R, Mo G, Luo S, Luo X, He L, Gonsamo A, Arabian J, Zhang Y *et al.* 2020. The global distribution of leaf chlorophyll content. *Remote Sensing of Environment* 236: 111479.
- Curran PJ. 1989. Remote sensing of foliar chemistry. *Remote Sensing of Environment* 30: 271–278.
- Dechant B, Cuntz M, Vohland M, Schulz E, Doktor D. 2017. Estimation of photosynthesis traits from leaf reflectance spectra: correlation to nitrogen content as the dominant mechanism. *Remote Sensing of Environment* 196: 279–292.
- Díaz S, Kattge J, Cornelissen JHC, Wright IJ, Lavorel S, Dray S, Reu B, Kleyer M, Wirth C, Colin Prentice I *et al.* 2016. The global spectrum of plant form and function. *Nature* 529: 167–171.
- Dietze MC, Serbin SP, Davidson C, Desai AR, Feng X, Kelly R, Kooper R, LeBauer D, Mantooth J, McHenry K *et al.* 2014. A quantitative assessment of a terrestrial biosphere model's data needs across North American biomes. *Journal of Geophysical Research-Biogeosciences* 119: 286–300.
- Domingues TF, Meir P, Feldpausch TR, Saiz G, Veenendaal EM, Schrodte F, Bird M, Djagbletey G, Hien F, Compaore H *et al.* 2010. Co-limitation of photosynthetic capacity by nitrogen and phosphorus in West Africa woodlands. *Plant, Cell & Environment* 33: 959–980.
- Elvidge CD. 1990. Visible and near infrared reflectance characteristics of dry plant materials. *International Journal of Remote Sensing* 11: 1775–1795.
- Ely KS, Burnett AC, Lieberman-Cribbin W, Serbin SP, Rogers A. 2019. Spectroscopy can predict key leaf traits associated with source-sink balance and carbon-nitrogen status. *Journal of experimental botany* 70: 1789–1799.
- Evans JR. 2021. Mesophyll conductance: walls, membranes and spatial complexity. *New Phytologist* 229: 1864–1876.
- Farquhar GV, von Caemmerer SV, Berry JA. 1980. A biochemical model of photosynthetic CO<sub>2</sub> assimilation in leaves of C<sub>3</sub> species. *Planta* 149: 78–90.
- Filzmoser P, Liebmann B, Varmuza K. 2009. Repeated double cross validation. *Journal of Chemometrics* 23: 160–171.
- Ghimire B, Riley WJ, Koven CD, Kattge J, Rogers A, Reich PB, Wright IJ. 2017. A global trait-based approach to estimate leaf nitrogen functional allocation from observations. *Ecological Application* 27: 1421–1434.
- Guanter L, Kaufmann H, Segl K, Foerster S, Rogass C, Chabrillat S, Kuester T, Hollstein A, Rossner G, Chlebek C *et al.* 2015. The EnMAP spaceborne imaging spectroscopy mission for earth observation. *Remote Sensing* 7: 8830–8857.
- Gui XJ, Lian JY, Zhang RJ, Li YP, Shen H, Ni YL, Ye WH. 2019. Vertical structure and its biodiversity in a subtropical evergreen broadleaved forest at Dinghushan in Guangdong Province, China. *Biodiversity Science* 27: 619–629 (in Chinese).
- He LM, Chen JM, Liu J, Zheng T, Wang R, Joiner J, Chou S, Chen B, Liu Y, Liu RG *et al.* 2019. Diverse photosynthetic capacity of global ecosystems mapped by satellite chlorophyll fluorescence measurements. *Remote Sensing of Environment* 232: 111344.
- He NP, Liu CC, Piao SL, Sack L, Xu L, Luo YQ, He JS, Han XG, Zhou GS, Zhou XH *et al.* 2019. Ecosystem traits linking functional traits to macroecology. *Trends in Ecology & Evolution* 34: 200–210.
- Jacquemoud S, Verhoef W, Baret F, Bacour C, Zarco-Tejada PJ, Asner GP, François C, Ustin SL. 2009. PROSPECT+SAIL models: a review of use for vegetation characterization. *Remote Sensing of Environment* 113: S56–S66.
- Jiang C, Ryu Y, Wang H, Keenan TF. 2020. An optimality-based model explains seasonal variation in C<sub>3</sub> plant photosynthetic capacity. *Global Change Biology* 26: 6493–6510.
- Kattge J, Knorr W, Raddatz T, Wirth C. 2009. Quantifying photosynthetic capacity and its relationship to leaf nitrogen content for global-scale terrestrial biosphere models. *Global Change Biology* 15: 976–991.
- Khan HA, Nakamura Y, Furbank RT, Evans JR. 2020. Effect of leaf temperature on the estimation of photosynthetic and other traits of wheat leaves from hyperspectral reflectance. *Journal of Experimental Botany* 72: 1271–1281.
- Kokaly RF, Asner GP, Ollinger SV, Martin ME, Wessman CA. 2009. Characterizing canopy biochemistry from imaging spectroscopy and its application to ecosystem studies. *Remote Sensing of Environment* 113: S78–S91.
- Koven CD, Knox RG, Fisher RA, Chambers JQ, Christoffersen BO, Davies SJ, Detto M, Dietze MC, Faybishenko B, Holm J *et al.* 2020. Benchmarking and parameter sensitivity of physiological and vegetation dynamics using the

- Functionally Assembled Terrestrial Ecosystem Simulator (FATES) at Barro Colorado Island, Panama. *Biogeosciences* 17: 3017–3044.
- Kumarathunge DP, Medlyn BE, Drake JE, Tjoelker MG, Aspinwall MJ, Battaglia M, Cano FJ, Carter KR, Cavaleri MA, Cernusak LA *et al.* 2019. Acclimation and adaptation components of the temperature dependence of plant photosynthesis at the global scale. *New Phytologist* 222: 768–784.
- Lebauer DS, Wang D, Richter JT, Davidson C, Dietze MC. 2013. Facilitating feedbacks between field measurements and ecosystem models. *Ecological Monographs* 83: 133–154.
- Liang XY, Liu S. 2019. *In-situ* measurement of photosynthetic characteristics of dominant tree species based on canopy crane in a Korean pine broad-leaved forest in Changbai Mountain, northeastern China. *Chinese Journal of Applied Ecology* 30: 1494–1502 (in Chinese).
- Luo XZ, Croft H, Chen JM, He LM, Keenan TF. 2019. Improved estimates of global terrestrial photosynthesis using information on leaf chlorophyll content. *Global Change Biology* 25: 2499–2514.
- Meacham-Hensold K, Montes CM, Wu J, Guan K, Fu P, Ainsworth EA, Pederson T, Moore CE, Brown KL, Raines C *et al.* 2019. High-throughput field phenotyping using hyperspectral reflectance and partial least squares regression (PLSR) reveals genetic modifications to photosynthetic capacity. *Remote Sensing of Environment* 231: 111176.
- Nakaji T, Oguma H, Nakamura M, Kachina P, Asanok L, Marod D, Aiba M, Kurokawa H, Kosugi Y, Kassim AR *et al.* 2019. Estimation of six leaf traits of East Asian forest tree species by leaf spectroscopy and partial least square regression. *Remote Sensing of Environment* 233: 111381.
- Niinemets Ü, Keenan TF, Hallik L. 2015. A worldwide analysis of within-canopy variations in leaf structural, chemical and physiological traits across plant functional types. *New Phytologist* 205: 973–993.
- Norby RJ, Gu LH, Haworth IC, Jensen AM, Turner BL, Walker AP, Warren JM, Weston DJ, Xu CG, Winter K. 2017. Informing models through empirical relationships between foliar phosphorus, nitrogen and photosynthesis across diverse woody species in tropical forests of Panama. *New Phytologist* 215: 1425–1437.
- Ollinger SV. 2011. Sources of variability in canopy reflectance and the convergent properties of plants. *New Phytologist* 189: 375–394.
- Ollinger SV, Smith ML. 2005. Net primary production and canopy nitrogen in a temperate forest landscape: an analysis using imaging spectroscopy, modeling and field data. *Ecosystems* 8: 760–778.
- Osnas JLD, Lichstein JW, Reich PB, Pacala SW. 2013. Global leaf trait relationships: mass, area, and the leaf economics spectrum. *Science* 340: 741–744.
- Prentice IC, Dong N, Gleason SM, Maire V, Wright IJ. 2014. Balancing the costs of carbon gain and water transport: testing a new theoretical framework for plant functional ecology. *Ecology Letters* 17: 82–91.
- Reich PB, Wright IJ, Lusk CH. 2007. Predicting leaf physiology from simple plant and climate attributes: a global GLOPNET analysis. *Ecological Applications* 17: 1982–1988.
- Ricciotto D, Sargsyan K, Thornton P. 2018. The impact of parametric uncertainties on biogeochemistry in the E3SM land model. *Journal of Advances in Modeling Earth Systems* 10: 297–319.
- Roberts DA, Ustin SL, Ogunjimiyo S, Greenberg J, Dobrowski SZ, Chen J, Hinckley TM. 2004. Spectral and structural measures of Northwest forest vegetation at leaf to landscape scales. *Ecosystems* 7: 545–562.
- Rogers A. 2014. The use and misuse of  $V_{c,max}$  in Earth system models. *Photosynthesis Research* 119: 15–29.
- Rogers A, Medlyn BE, Dukes JS, Bonan G, Caemmerer S, Dietze MC, Kattge J, Leakey ADB, Mercado LM, Niinemets Ü *et al.* 2017a. A roadmap for improving the representation of photosynthesis in Earth system models. *New Phytologist* 213: 22–42.
- Rogers A, Serbin SP, Ely KS, Sloan VL, Wullschlegel SD. 2017b. Terrestrial biosphere models underestimate photosynthetic capacity and  $CO_2$  assimilation in the Arctic. *New Phytologist* 216: 1090–1103.
- Scafareo AP, Xiang S, Long BM, Bahar NHA, Weerasinghe LK, Creek D, Evans JR, Reich PB, Atkin OK. 2017. Strong thermal acclimation of photosynthesis in tropical and temperate wet-forest tree species: the importance of altered Rubisco content. *Global Change Biology* 23: 2783–2800.
- Schimel D, Poulter B. 2021. The Earth in living color: monitoring our planet from above. *Eos* 102: doi: 10.1029/2021EO159404.
- Schimel D, Schneider FD, Carbon JPL, Participants E. 2019. Flux towers in the sky: global ecology from space. *New Phytologist* 224: 570–584.
- Schweiger AK. 2020. Spectral field campaigns: planning and data collection. In: Cavender-Bares J, Gamon JA, Townsend PA, eds. *Remote sensing of plant biodiversity*. Cham, Switzerland: Springer International Publishing, 385–423.
- Serbin SP, Dillaway DN, Kruger EL, Townsend PA. 2012. Leaf optical properties reflect variation in photosynthetic metabolism and its sensitivity to temperature. *Journal of Experimental Botany* 63: 489–502.
- Serbin SP, Singh A, McNeil BE, Kingdon CC, Townsend PA. 2014. Spectroscopic determination of leaf morphological and biochemical traits for northern temperate and boreal tree species. *Ecological Applications* 24: 1651–1669.
- Serbin SP, Singh A, Desai AR, Dubois SG, Jablonski AD, Kingdon CC, Kruger EL, Townsend PA. 2015. Remotely estimating photosynthetic capacity, and its response to temperature, in vegetation canopies using imaging spectroscopy. *Remote Sensing of Environment* 167: 78–87.
- Serbin SP, Townsend PA. 2020. Scaling functional traits from leaves to canopies. In: Cavender-Bares J, Gamon JA, Townsend PA, eds. *Remote sensing of plant biodiversity*. Cham, Switzerland: Springer, Chapter 3, 47–68.
- Serbin SP, Wu J, Ely KS, Kruger EL, Townsend PA, Meng R, Wolfe BT, Chlus A, Wang ZH, Rogers A. 2019. From the Arctic to the tropics: multibiome prediction of leaf mass per area using leaf reflectance. *New Phytologist* 224: 1557–1568.
- Shen T, Corlett RT, Song L, Ma WZ, Guo XL, Song Y, Wu Y. 2018. Vertical gradient in bryophyte diversity and species composition in tropical and subtropical forests in Yunnan, SW China. *Journal of Vegetation Science* 29: 1075–1087.
- Shiklomanov AN, Cowdery EM, Bahn M, Byun C, Jansen S, Kramer K, Minden V, Niinemets Ü, Onoda Y, Soudzilovskaia NA *et al.* 2020. Does the leaf economic spectrum hold within plant functional types? A Bayesian multivariate trait meta-analysis. *Ecological Applications* 30: 02064.
- Silva-Perez V, Molero G, Serbin SP, Condon AG, Reynolds MP, Furbank RT, Evans JR. 2018. Hyperspectral reflectance as a tool to measure biochemical and physiological traits in wheat. *Journal of Experimental Botany* 69: 483–496.
- Singh A, Serbin SP, McNeil BE, Kingdon CC, Townsend PA. 2015. Imaging spectroscopy algorithms for mapping canopy foliar chemical and morphological traits and their uncertainties. *Ecological Applications* 25: 2180–2197.
- Smith NG, Dukes JS. 2018. Drivers of leaf carbon exchange capacity across biomes at the continental scale. *Ecology* 99: 1610–1620.
- Smith NG, Keenan TF, Prentice IC, Wang H, Wright IJ, Niinemets Ü, Crous KY, Domingues TF, Guerrieri R, Yoko Ishida F *et al.* 2019. Global photosynthetic capacity is optimized to the environment. *Ecology Letters* 22: 506–517.
- Stavros EN, Schimel D, Pavlick R, Serbin S, Swann A, Duncanson L, Fisher JB, Fassnacht F, Ustin S, Dubayah R *et al.* 2017. ISS observations offer insights into plant function. *Nature Ecology and Evolution* 1: 0194.
- Thompson DR, Cawse-Nicholson K, Erickson Z, Ficht CG, Frankenberg C, Gao B-C, Gierach MM, Green RO, Jensen D, Natraj V *et al.* 2019. A unified approach to estimate land and water reflectances with uncertainties for coastal imaging spectroscopy. *Remote Sensing of Environment* 231: 111198.
- Uddling J, Gelang-Alfredsson J, Piikki K, Pleijel H. 2007. Evaluating the relationship between leaf chlorophyll concentration and SPAD-502 chlorophyll meter readings. *Photosynthesis Research* 91: 37–46.
- Ustin SL, Gitelson AA, Jacquemoud S, Schaepman M, Asner GP, Gamon JA, Zarco-Tejada P. 2009. Retrieval of foliar information about plant pigment systems from high resolution spectroscopy. *Remote Sensing of Environment* 113: S67–S77.
- Walker AP, Beckerman AP, Gu LH, Kattge J, Cernusak LA, Domingues TF, Scales JC, Wohlfahrt G, Wullschlegel SD, Woodward FI. 2014. The relationship of leaf photosynthetic traits- $V_{c,max}$  and  $J_{max}$  to leaf nitrogen, leaf phosphorus, and specific leaf area: a meta-analysis and modeling study. *Ecology and Evolution* 4: 3218–3235.
- Wang H, Harrison SP, Prentice IC, Yang YZ, Bai F, Togashi HF, Wang M, Zhou SX, Ni J. 2018. The China plant trait database: toward a comprehensive regional compilation of functional traits for land plants. *Ecology* 99: 500.

- Wang H, Prentice IC, Keenan TF, Davis TW, Wright IJ, Cornwell WK, Evans BJ, Peng CH. 2017. Towards a universal model for carbon dioxide uptake by plants. *Nature Plants* 3: 734–741.
- Wang S, Guan K, Wang ZH, Ainsworth EA, Zheng T, Townsend PA, Li KY, Moller C, Wu GH, Jiang CY. 2020. Unique contributions of chlorophyll and nitrogen to predict crop photosynthetic capacity from leaf spectroscopy. *Journal of Experimental Botany* 72: 341–354.
- Wold S, Sjöström M, Eriksson L. 2001. PLS-regression: a basic tool of chemometrics. *Chemometrics and Intelligent Laboratory Systems* 58: 109–130.
- Wright IJ, Reich PB, Westoby M. 2003. Least-cost input mixtures of water and nitrogen for photosynthesis. *The American Naturalist* 161: 98–111.
- Wright IJ, Reich PB, Westoby M, Ackerly DD, Baruch Z, Bongers F, Cavender-Bares J, Chapin T, Cornelissen JHC, Diemer M *et al.* 2004. The worldwide leaf economics spectrum. *Nature* 428: 821–827.
- Wright IJ, Reich PB, Cornelissen JHC, Falster DS, Groom PK, Hikosaka K, Lee W, Lusk CH, Niinemets Ü, Oleksyn J *et al.* 2005. Modulation of leaf economic traits and trait relationships by climate. *Global Ecology and Biogeography* 14: 411–421.
- Wu J, Albert LP, Lopes AP, Restrepo-Coupe N, Hayek M, Wiedemann KT, Guan K, Stark SC, Christoffersen B, Prohaska N *et al.* 2016. Leaf development and demography explain photosynthetic seasonality in Amazon evergreen forests. *Science* 351: 972–976.
- Wu JB, Guan DX, Sun XM, Zhang M, Shi TT, Han SJ, Jin CJ. 2006. Photosynthetic characteristics of dominant tree species and canopy in the broadleaved Korean pine forest of Changbai Mountains. *Science China Series D: Earth Sciences* 49: 89–98.
- Wu J, Rogers A, Albert LP, Ely K, Prohaska N, Wolfe BT, Oliveira RC Jr, Saleska SR, Serbin SP. 2019. Leaf reflectance spectroscopy captures variation in carboxylation capacity across species, canopy environment and leaf age in lowland moist tropical forests. *New Phytologist* 224: 663–674.
- Ye WH, Cao HL, Huang ZL, Lian JY, Wang ZG, Li L, Wei SG, Wang ZM. 2008. Community structure of a 20 hm<sup>2</sup> lower subtropical evergreen broadleaved forest plot in Dinghushan, China. *Chinese Journal of Plant Ecology* 32: 274–286 (in Chinese).
- Zarco-Tejada PJ, Miller JR, Mohammed GH, Noland TL. 2000. Chlorophyll fluorescence effects on vegetation apparent reflectance: I. Leaf-level measurements and model simulation. *Remote Sensing of Environment* 74: 582–595.
- Zhang Y, Joiner J, Gentine P, Zhou S. 2018. Reduced solar-induced chlorophyll fluorescence from GOME-2 during Amazon drought caused by dataset artifacts. *Global Change Biology* 24: 2229–2230.
- Zheng T, Chen J, He L, Arain MA, Thomas SC, Murphy JG, Geddes JA, Black TA. 2017. Inverting the maximum carboxylation rate ( $V_{cmax}$ ) from the sunlit leaf photosynthesis rate derived from measured light response curves at tower flux sites. *Agricultural and Forest Meteorology* 236: 48–66.

## Supporting Information

Additional Supporting Information may be found online in the Supporting Information section at the end of the article.

**Fig. S1** Example of demonstration of the response of net CO<sub>2</sub> assimilation rate ( $A$ ) to intracellular CO<sub>2</sub> concentration ( $C_i$ ) for the typical species at the three forest sites.

**Fig. S2** The leaf maximum carboxylation rate of RuBisCo standardised to 25°C ( $V_{c,max25}$ ) derived using the temperature response functions as described Bernacchi *et al.* (2013) is highly consistent with that derived using the site-specific temperature response functions as described Kumarathunge *et al.* (2019).

**Fig. S3** Example of demonstration of leaf reflectance spectra for the typical species from the three forest types.

**Fig. S4** Relationships of PROSPECT-5 inverted leaf chlorophyll (Chl) content with SPAD-based leaf chlorophyll content (Chl<sub>SPAD</sub>) and leaf maximum carboxylation rate of RuBisCo standardised to 25°C ( $V_{c,max25}$ ).

**Fig. S5** Histogram distributions of leaf traits under the controlled leaf age scenario (i.e. mature leaves only).

**Fig. S6** Exploring the trait– $V_{c,max25}$  relationships both within and across forest types under the mature leaf age scenario.

**Fig. S7** The selection criterion for the optimal number of latent variables in the spectral model of leaf maximum carboxylation rate of RuBisCo standardised to 25°C ( $V_{c,max25}$ ) under the cross-site scenario using partial least-squares regression (PLSR).

**Fig. S8** Histogram distribution of the coefficient of determination ( $R^2$ ) for the partial least-squares regression (PLSR) spectral models over the 200 repetitions under the cross-site scenario.

**Fig. S9** Accuracy assessments for the cross-site spectral models of leaf morphological and biochemical traits.

**Fig. S10** Comparisons between the observed and spectral-modelled trait– $V_{c,max25}$  relationships across the three forest types.

**Methods S1** The protocol for the  $A$ – $C_i$  curve (i.e. the response of net CO<sub>2</sub> assimilation rate ( $A$ ) to intracellular CO<sub>2</sub> concentration ( $C_i$ )) measurement.

**Table S1** The soil information of the three forest types in China.

**Table S2** Summary of species, leaf traits and sample size of representative canopy trees across the three forest types in China.

**Table S3** Statistical summary of the relationships between leaf maximum carboxylation rate of RuBisCo standardised to 25°C ( $V_{c,max25}$ ) and the four leaf morphological and biochemical traits across the three forest types.

Please note: Wiley Blackwell are not responsible for the content or functionality of any Supporting Information supplied by the authors. Any queries (other than missing material) should be directed to the *New Phytologist* Central Office.